Title: Trapping of Nicotinic Acetylcholine Receptor Ligands Assayed by *in vitro* Cellular Studies and *in vivo* PET Imaging

Abbreviated Title: Trapping Hypothesis of Nicotine Addiction

Authors: Hannah J. Zhang[1], Chien-Min Kao[1], Matthew Zammit[1], Anitha P Govind[2], Samuel Mitchell[1], Nathanial Holderman[1], Mohammed Bhuiyan[1], Richard Freifelder[1], Xiaoxi Zhuang[2], Jogeshwar Mukherjee[3*], Chin-Tu Chen[1*], William N. Green[2*]

[1]Department of Radiology, University of Chicago, 5841 S Maryland Avenue, Chicago, IL 60637

[2]Department of Neurobiology, University of Chicago, 5841 S Maryland Avenue, Chicago, IL 60637

[3]Department of Radiological Sciences, University of California, Irvine, CA 92697.

Number of pages: 28

Number of figures, tables, multimedia, and 3D models: 5, 2, 0, 0.

Number of words for abstract, introduction, and discussion: 250, 559, 1496

Declaration of interests: The authors declared no conflict interests or competing financial interests.

Acknowledgements: This study was supported in part by the NIH grant R01 DA044760-01 to J.M., C.C. and W.N.G., RF1 AG029479 to J.M., and T32 DA043469 to M.Z. The authors acknowledge the assistance from the Integrative Small Animal Imaging Research Resources (iSAIRR) supported in part by the NIH grant P30 CA14500 and S10 OD025265, and from the Cyclotron Facility of the University of Chicago.

*J.M., C.C., and W.N.G. equally supervised this work.

Correspondence should be addressed to Chin-Tu Chen at c-chen@uchicago.edu or William N. Green at wgreen@uchicago.edu

Abstract

A question relevant to nicotine addiction is how nicotine and other nicotinic receptor membrane-permeant ligands, such as the anti-smoking drug varenicline (Chantix), distribute in the brain. Previously, we found that varenicline is trapped in intracellular acidic vesicles that contain α4β2-type nicotinic receptors (α4β2Rs). Nicotine is not trapped but concentrates there. Here, combining subcellular methods with *in vivo* PET imaging, we present evidence that the α4β2R PET ligand, 2-FA85380 (2-FA), is trapped within α4β2R-containing acidic vesicles, while the PET ligand, Nifene, is not trapped. Additional evidence, using a fluorescent-tagged α4β2R PET ligand, Nifrolidine, identified the trapping vesicles as Golgi satellites, an organelle regulated by nicotine in neurons where α4β2Rs are expressed and traffics and processes α4β2Rs in those neurons. Using PET imaging, 2-[^{18}F]FA kinetics in high α4β2R-expressing regions were much slower than ligand unbinding rates consistent with 2-FA trapping in Golgi satellites extending ligand residence time and 2-[^{18}F]FA imaging of the Golgi satellites. Chloroquine, which dissipates acidic organelle pH gradients, reduced 2-[^{18}F]FA distribution in vivo consistent with ligand trapping. In contrast, [^{18}F]Nifene kinetics were rapid, consistent with ligand residence time reflecting ligand unbinding rates, and [^{18}F]Nifene imaging all α4β2R pools. Specific 2-[^{18}F]FA and [^{18}F]Nifene signals were eliminated in β2 subunit knockout mice or by acute nicotine injections demonstrating binding to high-affinity sites on β2-containing receptors. Altogether, we find that kinetic differences in α4β2R PET ligands are consistent with their distribution among different α4β2R pools in the brain, [^{18}F]Nifene binding and imaging all ligand-binding α4β2Rs and 2-[^{18}F]FA imaging α4β2Rs in Golgi satellites.

Significance

Mechanisms of nicotine addiction remain poorly understood. An earlier study using in vitro methods found that the anti-smoking nicotinic ligand, varenicline (Chantix) was trapped in α4β2R-containing acidic vesicles. Using a fluorescent labeled high-affinity nicotinic ligand, this study provided evidence that these intracellular acidic vesicles were α4β2R-containing Golgi satellites. *In vivo* PET imaging with F-18 labeled nicotinic ligands provided additional evidence that differences in PET ligand trapping in acidic vesicles were the cause of differences in PET ligand kinetics and subcellular distributions. These findings combining *in vitro* and *in vivo* imaging revealed new mechanistic insights into the kinetics of weak base PET imaging ligands and the subcellular mechanisms underlying nicotine addiction.

Introduction

Tobacco use continues world-wide and is the leading cause of preventable deaths in the United States (U.S. Department of Health and Human Services 2014). Nicotine, the addictive molecule in tobacco, binds to high-affinity nicotinic acetylcholine receptors (nAChRs) in the brain, where it initiates its addictive effects. nAChRs are members of the Cys-loop family of ligand-gated ion channels, all of which are pentameric neurotransmitter receptors (Karlin 2002, Albuquerque, Pereira et al. 2009). In mammalian brains, high-affinity nicotine binding sites are largely nAChRs containing α4 and β2 subunits (α4β2Rs) (Albuquerque, Pereira et al. 2009). In mice, knockout of either subunit reduced the pharmacological and behavioral effects of nicotine (Picciotto, Zoli et al. 1998, Marubio, Gardier et al. 2003), and this effect can be rescued by targeted β2 subunit expression in the mid-brain reward ventral tegmental area (VTA); (Maskos, Molles et al. 2005).

Chronic nicotine exposure causes α4β2R upregulation, a complex set of long-term changes causing both increases in α4β2R high-affinity binding site numbers and functional upregulation, the increased α4β2R functional response after nicotine exposure (Marks, Burch et al. 1983, Schwartz and Kellar 1983, Benwell, Balfour et al. 1988, Breese, Adams et al. 1997). Several other studies link the process of nicotine-induced α4β2R upregulation to nicotine addiction (Vezina, McGehee et al. 2007, Govind, Vezina et al. 2009, Govind, Walsh et al. 2012, Lewis and Picciotto 2013). Nicotine and other weak-base ligands of α4β2Rs, unlike acetylcholine, are highly membrane-permeant and rapidly reach equilibrium in intracellular organelles and concentrate in acidic organelles (Brown and Garthwaite 1979). The anti-smoking drug, varenicline (Chantix), is selectively trapped as a weak base within intracellular acidic vesicles that contain high-affinity α4β2Rs (Govind, Vallejo et al. 2017). Trapping maintains levels of varenicline for days in the brain after nicotine levels decline. Nicotine upregulation amplifies varenicline trapping by increasing the number of high-affinity binding sites, which increases the capacity of the acidic vesicles to trap varenicline and increasing acidic vesicle numbers.

Here we address whether the distribution of PET tracers used to assay α4β2Rs *in vivo*, which are weak bases, are affected by trapping in α4β2R-containing acidic vesicles. Because of the limits of PET image resolution, we performed *in vitro* cell binding competition assays to assess ligand trapping, which allow subcellular resolution using the same PET ligands. We present evidence that 2-FA85380 (2-FA) used as a PET tracer is trapped in α4β2R-containing acidic vesicles similar to varenicline trapping while Nifene is not trapped. The identity of α4β2R-containing acidic vesicles is unknown. Recently, we found that a novel intracellular compartment in neurons, Golgi satellites (GSats), contain high levels of α4β2Rs and GSats numbers are increased by nicotine exposure as well as increased neuronal activity (Govind, Jeyifous et al. 2021). Using a fluorescent-tagged α4β2R ligand, Nifrorhodamine, to image the subcellular localization of α4β2Rs, we present evidence that α4β2Rs accumulate in acidic vesicles that are GSats. Live PET imaging in mice using [^{18}F]Nifene and 2-[^{18}F]FA were consistent with *in vitro* results with the kinetics of 2-[^{18}F]FA PET signals were much slower than that of [^{18}F]Nifene consistent with 2-[^{18}F]FA being trapped in acidic vesicles. Chloroquine, which dissipates the pH gradient across acidic organelles, reduced trapping *in vitro* and reduced 2-[^{18}F]FA's distribution volume ratios (DVR) in midbrain and thalamus. Altogether, we conclude that 2-FA is trapped and images α4β2Rs in Golgi satellites while Nifene images all ligand-binding α4β2Rs because it is not confined to Golgi satellites.

Material and Methods

Cellular Binding Competition Assay

HEK cells stably expressing α4β2Rs were treated with 10 μM nicotine overnight. Cells were then washed four times with PBS, scraped off the plates, and suspended in PBS. Aliquots of cells were incubated with indicated concentrations of 2-FA, Nifene or nicotine respectively for 5 min followed by

addition of 2.5 nM [^{125}I]-epibatidine ([^{125}I]Epb) (2200 Ci/mmol; Perkin Elmer) and incubation for 20 min at room temperature. At the end of incubation, cells were harvested on Whatman GF/B filters presoaked in 0.5% polyethyleneimine and washed four times with PBS using a 24-channel cell harvester (Brandel, MD). Non-specific binding was estimated by incubating parallel samples in 1 mM nicotine with [^{125}I]Epb. Radioactivity of bound [^{125}I]Epb was determined using a gamma counter (Wallac, Perkin Elmer, MA). The binding of [^{125}I]Epb was normalized to the binding of cells without 2-FA, Nifene or nicotine treatment and plotted as percent of untreated cells.

Mammalian cell culture

Stable cell line expressing rat α4β2 nAChRs in HEK cells are from our lab, expressing untagged α4 and C-terminal, HA epitope-tagged β2 subunits (Vallejo, Buisson et al. 2005). Cell lines were maintained in DMEM (Gibco, Life technologies) with 10% calf serum (Hyclone, GE Healthcare Life Sciences, UT) at 37°C in the presence of 5% CO_2. DMEM was supplemented with Hygromycin (Thermofisher scientific, MA) at 0.4 mg/ml for maintaining selection of α4β2 HEK cells. Stable cells were plated in media without hygromycin for experiments.

Primary neuronal culture and transfections

Primary cultures of rat cortical neurons were prepared as described (Govind, Walsh et al. 2012) using Neurobasal Media (NBM), 2% (v/v) B27, and 2 mM L-glutamine (all from Thermofisher Scientific, MA). Dissociated cortical cells from E18 Sprague Dawley rat pups were plated on slips or plates coated with poly-D-lysine (Sigma, MO). For live imaging, neurons were plated in 35 mm glass bottom dishes (MatTek, MA). Cells were plated at a density of $0.25X10^6$ cells/mL on 35 mm dishes or per well in a 6-well plate. Neuronal cultures were transfected at DIV 10 with the Lipofectamine 2000 transfection reagent (Thermofisher Scientific, MA) according to manufacturer's recommendations. Neurons were transfected with cDNAs of α4, $\beta2_{HA}$ and Golgi markers, St3 GFP or St3 Halo. 0.5 μg of

each DNA up to a total of 1.5 μg were used per 35 mm imaging dish or per well of a 6 well plate. 24 hours after transfection, neurons were treated with 1 μM nicotine for 17 hrs.

Ligand treatment and ^{125}I-epibatidine binding

α4β2R HEK cells were treated with 10 μM nicotine, 100 μM Nifene, 100 μM 2-FA for 17 hours at 37°C in medium. Information for each ligand is displayed in Table 1. Cells were washed four times with PBS and collected by scrapping off from the plates using a cell scraper with PBS, resuspended in 1ml PBS. 1/20th of the cell suspension was distributed to three tubes followed by incubation in 2.5 nM [^{125}I]-Epb for 15 minutes. For competition experiments, intact cells were preincubated in the indicated concentrations of Nifene, 2-FA or nicotine for 5 min, followed by the addition of 2.5 nM [^{125}I]-Epb for 15 min. All binding was terminated by vacuum filtration through Whatman (Clifton, NJ) GF/B filters presoaked in 0.5% polyethyleneimine using a Brandel (Gaithersburg, MD) 24 channel cell harvester. Bound [^{125}I]-Epb (2200 Ci/mmol) was determined by γ counting (PerkinElmer Wallac, Gaithersburg, MD) with nonspecific binding estimated by [^{125}I]-Epb binding to cells that were preincubated with 1mM nicotine prior to epibatidine binding.

Altering intracellular pH of acidic intracellular organelles

Intact cells were treated with nAChR ligands for 17 hours and washed twice with PBS. Cells were exposed to two 5 min incubations with PBS containing 15, 150 μM chloroquine or 20 mM NH_4Cl to neutralize the pH of intracellular organelles and washed two times with PBS. Cells were gently scraped from the plates, re-suspended in PBS and subjected to [^{125}I]-Epb binding as described above.

Immunocytochemistry

Live labeling experiments were performed on cultured neurons grown in imaging chambers (MaTek), transfected with nAChR subunits α4 and β2 and Golgi markers, St3GFP or St3 Halo for 24 hours and

treated with 1 μM nicotine for 17 hours. Neurons were labeled with 25 μM Nifrorhodamine (analog of Nifrofam, Samra et al. 2018) or pHRodo (Thermofisher) as per manufacturers instruction for 30 minutes, washed three times with low fluorescence Hibernate E buffer (Brain Bits, IL) and imaged live in the same buffer. For total β2 staining, neurons were grown on coverslips, fixed with 4% paraformaldehyde + 4% sucrose for 10 minutes and permeabilized with 0.1% triton X100. β2 subunits were imaged by labeling the cells with mouse anti-HA antibody (1:500, Biolegend). Primary antibody incubations were for 1 hour and secondary antibodies for 45 minutes unless otherwise mentioned. Coverslips were mounted using Prolong Gold mounting media with DAPI. Fluorescence images were acquired using a Marianas Yokogawa type spinning disk confocal microscope with back-thinned EMCCD camera. Images were processed and analyzed using ImageJ/Fiji (US National Institutes of Health).

Animals

The male and female β2 nAChR knockout mice (KO) and their wild type (WT) littermates were generated in house by breeding a heterozygous pair on the C57BL/6J background purchased from the Jackson Lab (Bar Harbor, ME) (Picciotto, Zoli et al. 1995). Additional male and female WT mice at the same age were purchased directly from the Jackson lab and used in the same manner as the WT littermates. Animals were housed in The University of Chicago Animal Research Resources Center. The Institutional Animal Care and Use Committee of the University of Chicago, in accordance with National Institutes of Health guidelines, approved all animal procedures. Mice were maintained at 22–24°C on a 12:12-h light-dark cycle and provided food (standard mouse chow) and water ad libitum. Mice aged between 3 and 10 months were used in this study. The number of the animals and their body weights are summarized in Table 2

Acute Nicotine Supplement

To demonstrate the binding specificity of weak base ligands, acute nicotine (AN) administration was performed to a group of WT mice. Nicotine ditartarte (Sigma-Aldrich, St Louis, MO) was prepared in isotonic saline at the concentration of 0.1 mg/ml freshly and filtered through a 0.2 µm syringe filter. Each mouse was injected 0.5 mg/kg body weight (BW) of nicotine intraperitoneally 15 min before the tracer administration and PET imaging according to the imaging protocol describe in the following sections.

Chloroquine Treatment

Chloroquine diphosphate (CQ) (Sigma-Aldrich, St Louis, MO) was dissolved in PBS and filtered through a 0.2 µm syringe filter. WT mice were used in the CQ treatment group (CQWT). Each mouse received 50 mg/kg BW/day of CQ by intraperitoneal injection for 3 days (Vodicka, Lim et al. 2014). Ten minutes after the third CQ injection, animals underwent 2-[^{18}F]FA administration and PET imaging according to the imaging protocol described in following sections.

Radiotracer Syntheses

Syntheses of both 2-[^{18}F]FA and [^{18}F]Nifene, two radiotracers for α4β2Rs, were carried out at the Cyclotron Facility of The University of Chicago. 2-[^{18}F]FA was synthesized from the commercially available precursor, 2-TMA-A85380. The [^{18}F]Nifene was synthesized from the precursor N-BOC-nitroNifene. An IBA Synthera V2 automatic synthesis module equipped with Synthera preparative HPLC was used for the radiolabeling and purification inside a Comecer hot cell. Typical yield for 2-[^{18}F]FA was 34% (decay corrected) with specific activities >3,000 mCi/µmole and radiochemical purity > 99%. The representative radiochemical yield was 6.3% (decay corrected) with specific activities >3,000 mCi/µmole and > 99% purity for [^{18}F]Nifene.

PET/CT Imaging

The imaging protocols were designed based on previous reports for 2-[^{18}F]FA and [^{18}F]Nifene (Horti, Chefer et al. 2000, Pichika, Easwaramoorthy et al. 2006, Constantinescu, Garcia et al. 2013) and our preliminary experiments fine-tuning the protocol (data not shown). An intraperitoneal (IP) catheter was placed at the lower right abdominal area of each mouse before the imaging. The animal was then placed into the β-Cube preclinical microPET imaging system (Molecubes, Gent, Belgium) in a small animal holder. The tracer was delivered in 200 μL isotonic saline via the IP catheter at the same time when the PET imaging starts and followed by flashing 100 μL of fresh saline. The injected doses were summarized in Table 2. Whole body imaging was acquired with 133 mm x 72 mm field of view (FOV) and an average spatial resolution of 1.1 mm at the center of FOV (Krishnamoorthy, Blankemeyer et al. 2018). List-mode data was recorded for three hour for 2-[^{18}F]FA and one hour for [^{18}F]Nifene followed by a reference CT image on the X-Cube preclinical microCT imaging system, (Molecubes, Gent, Belgium). The images were reconstructed using an OSEM reconstruction algorithm that corrected for attenuation, randoms and scatter with an isotropic voxel size of 400 μm and a re-binned frame rate of 18 x10 minutes for 2-[^{18}F]FA and 6 x10 minutes for [^{18}F]Nifene. CT images were reconstructed with a 200 μm isotropic voxel size and used for anatomic co-registration, scatter correction and attenuation correction. Animals were maintained under 1-2% isoflurane anesthesia in oxygen during imaging. Respiration and temperature were constantly monitored and maintained using the Molecubes monitoring interface, and Small Animal Instruments (SAII Inc, Stoney Brook, NY) set up. All animals survived the imaging.

Data Analyses of Tracer Uptake

To quantify the brain tracer uptake, analyses of CT-fused PET images were performed using VivoQuant software (Invicro, Boston, MA). Dynamic tracer uptake was analyzed and expressed in

standardized uptake value (SUV) in multiple 10-minute frames to generate time active curve (TAC) (Keyes 1995, Huang 2000, Hesterman, Ghayoor et al. 2019):

$$\mathrm{SUV} = \frac{\text{radioactivity concentration in volume of interest (VOI)} \left(\frac{\mu\mathrm{Ci}}{\mathrm{ml}}\right)}{\frac{\text{injected dose } (\mu\mathrm{Ci})}{\text{body weight of animal (g)}}}$$

Brain regional analysis was done using a 3-dimensional mouse brain atlas available as the VivoQuant software plug-in. The 3D brain atlas is based on the Paxinos-Franklin atlas registered to a series of high-resolution magnetic resonance imaging with 100 µm near isotropic data and has been applied in other studies (Slavine, Kulkarni et al. 2017, Hesterman, Ghayoor et al. 2019, Mazur, Powers et al. 2019). The brain was segmented into 14 regions within the skull of each animal using the CT as the reference for automatic registration. Among the 14 regions, 6 regions (cerebellum, cortex, hippocampus, midbrain, striatum, and thalamus) that represent the high, middle and low nicotinic receptor levels in the brain are presented in this study. The small size of some brain regions (e.g., hippocampus), partial volume effects and activity spillover from neighboring regions may lead to some under or over estimation of radiotracer when using the software to extract the volumes-of-interest (VOI). The VOI of the whole brain was 473±3.39 mm^3 (mean±SEM).

Distribution volume ratio calculation

PMOD kinetic modeling software (Bruker, Zürich, Switzerland) was used to compute the distribution volume ratio (DVR) of the thalamus and midbrain of each mouse using Logan graphical analysis (Logan, Fowler et al. 1996) with the cerebellum used as the reference region. Using the concentration TACs generated from the VOIs from the Vivoquant brain atlas, a simplified reference tissue model (SRTM) was used to compute the $k_2{}'$ value for each region. Then a Logan plot was created, and the slope used as the DVR.

Statistical Analyses

Statistical analyses were performed using Prism software (GraphPad, La Jolla, CA, USA). Continuous data were summarized as mean with standard errors with statistically significant differences assessed using t-test between two groups and one-way and two-way ANOVA among multiple groups. $p<0.05$ was considered statistically significant.

Results

Trapping of α4β2R PET ligands in α4β2R-containing intracellular acidic vesicles

Using HEK cells stably expressing α4β2Rs, we performed competitive binding of different ligands using [^{125}I]-Epb binding to α4β2Rs expressed in HEK cells to estimate relative affinities of the PET ligands, Nifene and 2-FA (see structure in Fig 1 A), and with that of nicotine. The Ki values from the fits to the data (Fig 1 B) were 7.1 x10^{-11} M for 2-FA, 3.1x10^{-10} for Nifene and 9.4 x10^{-10} for nicotine indicating that Nifene has a higher affinity for α4β2R binding sites than nicotine, and 2-FA a higher affinity than Nifene. These estimates (Table 1) of 2-FA and Nifene affinities for α4β2R binding sites together with their pKa values (Hansch, Corwin et al. 1995, Davila-Garcia, Musachio et al. 1997, Valette, Bottlaender et al. 1999, Brown, Chefer et al. 2004, Pichika, Easwaramoorthy et al. 2006, Lu, Chen et al. 2007, Gao, Kuwabara et al. 2008, Govind, Vallejo et al. 2017, Thompson, Metzger et al. 2017, Mukherjee, Lao et al. 2018) suggest that 2-FA and Nifene could become trapped in α4β2R-containing intracellular acidic vesicles similar to varenicline and epibatidine.

To assay for the trapping of Nifene and 2-FA in α4β2R-containing intracellular acidic vesicles, we measured the degree to which overnight (17 hour) exposure to the ligand increased the number of high-affinity α4β2R binding sites using [^{125}I]-Epb binding, which is a measure of α4β2R upregulation by the ligand. If the assay is performed on live HEK cells expressing α4β2Rs, varenicline (Fig. 1C) and epibatidine (Govind, Vallejo et al. 2017) do not cause any significant upregulation compared to the 5-

fold upregulation with nicotine exposure (Fig. 1C). However, if the assay is performed using membranes prepared from the cells in which intracellular acidic vesicles are not intact, α4β2R upregulation by varenicline and epibatidine is similar to that by nicotine (Govind, Vallejo et al. 2017). These data are consistent with varenicline and epibatidine being concentrated and trapped within the α4β2R-containing intracellular acidic vesicles, thereby preventing [^{125}I]-Epb binding because varenicline and epibatidine are occupying the α4β2R binding sites in the vesicle lumen. Like varenicline, α4β2Rs were not upregulated by 2-FA for live HEK cells (Fig. 1C). In contrast, α4β2Rs were upregulated by Nifene almost to the same degree as upregulation by nicotine (Fig. 1C). These findings suggest that 2-FA is trapped within α4β2R-containing intracellular acidic vesicles similar to varenicline while Nifene is largely not trapped.

Upregulation by varenicline and epibatidine could be partially restored for live HEK cells by different treatments that dissipated the pH gradient across the vesicle membrane. These included the addition of a weak base that is not a α4β2R ligand, chloroquine (CQ) or ammonium chloride (NH_4Cl). Consistent with 2-FA trapping within α4β2R-containing intracellular acidic vesicles, both chloroquine at 15 or 150 μM and ammonium chloride at 20 mM increased the effects of 2-FA and varenicline in terms of the upregulation of α4β2Rs in the HEK cells (Fig. 1D).

Are α4β2R-containing intracellular acidic vesicles Golgi satellites?

We have recently characterized changes in the Golgi apparatus that occur with nicotine exposure and parallel upregulation of α4β2Rs (Govind, Jeyifous et al. 2021). With nicotine exposure, small organelles, Golgi satellites, form out of the endoplasmic reticulum (ER). Golgi satellite formation only occurs in response to nicotine when α4β2Rs are expressed in HEK cells or in neurons and the effects of nicotine are reversible. Golgi satellites had not been characterized previously because the usual Golgi markers used to image Golgi are Golgi structural proteins that are not found in Golgi satellites

(Govind, Jeyifous et al. 2021). To examine whether the α4β2R-containing intracellular acidic vesicles are Golgi satellites we used the Golgi enzyme sialyltransferase Gal3 (St3) which label Golgi Satellites in addition to the Golgi apparatus. In Fig. 2, we expressed a GFP-tagged version of St3 in cultured rat cortical neurons together with α4 and HA-tagged β2 subunits.

As shown in Fig. 2, St3-GFP labels the Golgi apparatus found in the soma (Fig. 2A) of the neurons that have been exposed to nicotine for 17 hours, which increases the numbers of Golgi satellites (Govind, Jeyifous et al. 2021). St3-GFP also labels smaller structures that are the Golgi satellites and extend out into the neuronal processes. Two different examples of neurons are displayed in Fig. 2A both expressing St3-GFP (green), but with the α4β2Rs labeled using different probes. In the top image, the α4β2Rs were labeled with fluorescent anti-HA antibody. This probe labels all β2 subunits with most of the staining found in the soma in what appears to be the ER where β2 subunits are synthesized and assemble with α4 into α4β2Rs (Sallette, Pons et al. 2005). The probe also stains the Golgi apparatus but appears to have little overlap with the smaller St3 puncta, which are the Golgi satellites. This apparent lack of overlap results from the extremely bright staining of the β2 subunits in the ER relative to β2 subunit staining of the Golgi satellites. The presence of β2 subunits in Golgi satellites is better observed in dendrites (Fig. 2B) where the levels of ER are much smaller, and consequently, staining of β2 subunits in ER is much weaker. Thus, the overlap between labelled β2 subunits and St3 labeling of Golgi satellites is apparent in dendrites (compare Fig. 2B images in the left panels).

In Fig. 2A bottom, α4β2Rs labeled using membrane-permeable, Nifrorhodamine, that binds to α4β2R high-affinity binding sites and is an analogue of Nifrolidine, used in α4β2R PET imaging (Chattopadhyay, Xue et al. 2005). Surprisingly, Nifrorhodamine labeling does not colocalize with β2 subunit staining in the ER or Golgi apparatus (GA) in the soma. Instead, Nifrorhodamine labeling co-localizes with the Golgi satellites labeled with St3-GFP in the soma and dendrites (center panels).

These findings suggest that a α4β2R high-affinity binding site form in Golgi satellites and not during assembly in the ER. Shown in the right panels of Fig. 2B are dendrites expressing St3-GFP and labeled with pHrodo, a fluorescent probe that fluoresces at pH values found in acidic vesicles. PHrodo fluorescence overlays with a significant number of the St3-positive puncta as well as other acidic organelles consistent with mature Golgi satellites being acidic vesicles.

PET studies with 2-[^{18}F]FA and [^{18}F]Nifene

To understand the binding kinetics of α4β2Rs ligands *in vivo*, 2-[^{18}F]FA and [^{18}F]Nifene were used for brain PET imaging in mice. Figure 3A displayed typical brain images of 2-[^{18}F]FA and [^{18}F]Nifene binding at coronal, sagittal, and transverse sections of the brain in WT mice. Whole brain uptake of [^{18}F]Nifene was significantly greater than 2-[^{18}F]FA as seen in Fig-3A. The TACs of the whole brain from the WT mice for 2-[^{18}F]FA and [^{18}F]Nifene are shown in Figure 3B. [^{18}F]Nifene demonstrated fast kinetics peaking at ~10 minutes with a SUV of ~1.6 after tracer injection. In contrast the binding of 2-[^{18}F]FA was slower peaking at ~50 minutes with a SUV of ~0.6. The significant difference in brain kinetics between the two radiotracers is seen in the inset of Fig-3B where whole brain [^{18}F]Nifene reduces to below 50% levels within 40 mins whereas 2-[^{18}F]FA remained at ~70% of the peak at the end of 3 hour imaging time.

The whole brain retention for both 2-[^{18}F]FA and [^{18}F]Nifene was significantly decreased in the β2 KO mice. This is similar to our previous observations of a lack of [^{18}F]Nifene binding in β2 KO mice (Bieszczad, Kant et al. 2012). Similarly, 2-[^{18}F]FA cleared from the β2 KO mice brain more rapidly, with SUV values reduced by approximately 50% of WT animals at 3 hrs post-injection (Fig-3C). Reductions in whole brain SUV of [^{18}F]Nifene were also approximately 50% in the β2 KO mice compared to WT animals (Fig-3D).

Acute nicotine challenge in WT animals affected the whole brain uptake and retention of both 2-[^{18}F]FA and [^{18}F]Nifene. The initial higher uptake of both 2-[^{18}F]FA and [^{18}F]Nifene compared to the KO mice may be due to the higher free fraction caused by the nicotine challenge. In the case of 2-[^{18}F]FA, acute nicotine brought the SUV levels at the end of the 3 hr scan similar to the β2 KO mice brain (Fig-3C). Retention of [^{18}F]Nifene after acute nicotine was similarly reduced with clearance profile similar to that found in the β2 KO mice brain (Fig-3D).

[^{18}F]Nifene Binding in Brain Regions

Regional brain distribution of [^{18}F]Nifene binding was analyzed in the thalamus, midbrain, hippocampus, striatum, cortex and cerebellum. In wild type mice, [^{18}F]Nifene showed the highest SUV in the thalamus and midbrain and the lowest SUV in the cerebellum throughout the imaging duration (Fig 4A). Time activity curves in the various regions followed a similar profile in all brain regions. Levels of [^{18}F]Nifene binding in the β2 KO mice brain were reduced to the level of cerebellum in all regions (Fig 4B). In the case of acute nicotine administration initial levels of uptake were higher than β2 KO mice (Fig 4C), which may be due to higher free fraction of [^{18}F]Nifene, but subsequently retention of [^{18}F]Nifene was not observed in receptor rich regions, unlike the WT without nicotine (Fig 4A).

Using cerebellum as the reference region, DVR of [^{18}F]Nifene in the three groups of mice are shown for the thalamus (Fig 4D) and mid-brain (Fig 4E). The DVR values for β2 KO mice and acute nicotine treated mice were <1. The wild type mice had DVR approaching 2 in the thalamus and over 1.6 in the midbrain. Differences between the wild type and β2 KO mice were highly significant, as well as the difference between wild type and acute nicotine treated animals. The similar DVR levels of β2 KO

mice and acute nicotine treated animals confirms the apparent lack of receptor-mediated specific binding.

2-[^{18}F]FA Binding in Brain Regions

In WT mice, 2-[^{18}F]FA showed the highest SUV (~0.7) in the thalamus and midbrain and the lowest SUV in the cerebellum (~0.2-0.3) at the end of the imaging session (Fig 5A). Other regions such as the striatum and cortex exhibited moderate levels of 2-[^{18}F]FA binding. All brain regions in the β2 KO mice exhibited a similar uptake and clearance profile with SUV values similar to cerebellum of ~0.2-0.3 (Fig 5B). Similarly, acute nicotine was also able to block retention of 2-[^{18}F]FA binding in various brain regions with SUV values similar to cerebellum of ~0.3 (Fig 5C).

Because cerebellum had the lowest levels of 2-[^{18}F]FA, DVR in other regions used cerebellum as the reference region. Thalamus had the highest DVR (>2) in WT mice followed by midbrain DVR (~2) (Fig 5G, H). The DVR values for β2 KO mice and acute nicotine treated mice were <1. Differences between the wild type and β2 KO mice were highly significant, as well as the difference between wild type and acute nicotine treated animals. The similar DVR levels of β2 KO mice and acute nicotine treated animals confirms the apparent lack of receptor-mediated specific binding.

To further test whether the mechanism causing 2-[^{18}F]FA slow kinetics, mice were treated with CQ, which as discussed previously, dissipates the pH gradient across acidic organelles and reduced trapping *in vitro* (Fig. 1D; (Govind, Vallejo et al. 2017)). Previous studies had established that the maximum amount of CQ that can be injected into mice resulted in blood level of ~15 μM CQ for 3 days before PET imaging with 2-[^{18}F]FA. Increased uptake of 2-[^{18}F]FA was observed in several brain regions post CQ treatment. This increase in 2-[^{18}F]FA uptake may reflect an effect on the ability of 2-

[^{18}F]FA to sequester in intracellular acidic vesicles throughout the brain, which would increase levels of free 2-[^{18}F]FA. Compared to the regional binding difference in WT mice (Fig 5A), CQ reduced the regional differences of 2-[^{18}F]FA binding although the nonspecific 2-[^{18}F]FA binding increased in CQWT mice (Fig 5D). This reduction in specific binding to α4β2Rs is more evident in the binding ratios of different regions to cerebellum (Fig 5E and 5F). Binding of 2-[^{18}F]FA in thalamus of the WT animals is approximately 2.5 fold over that in cerebellum at the end of 3 hour imaging, while it is less than 1.5 fold in CQ treated animals. Similarly, binding of 2-[^{18}F]FA in other brain regions were also reduced. The decrease in thalamic and mid-brain DVR of CQ treated mice were statistically significant (Fig 5G and 5H). Thus, the results demonstrate that CQ treatment of the mice significantly reduced the specific 2-[^{18}F]FA signal in the thalamus and midbrain consistent with it reducing 2-FA trapping as we observed *in vitro* (Fig. 1D).

Discussion

Despite the known adverse consequences associated with smoking, smoking cessation is difficult. Even with the most effective smoking cessation reagent, varenicline, quitting rates reach only ~50% (Agboola, Coleman et al. 2015). To rationally design better smoking cessation drugs, it is critical to understand the molecular and cellular mechanisms governing how drugs dampen the effects of nicotine on the brain's reward pathway. Varenicline was designed as a high-affinity, partial agonist that mediates anti-smoking effects through acute, rapid interactions with α4β2Rs that reduce the full-agonist effects of nicotine. Our lab has discovered additional long-term effects of varenicline in which varenicline is trapped in intracellular acidic vesicles and maintain brain levels throughout the day, importantly, after nicotine levels decline (Govind, Vallejo et al. 2017). We demonstrated that the slow release of trapped varenicline reduced the functionally upregulated α4β2R currents, which should contribute to varenicline effects on smokers (Govind, Vallejo et al. 2017).

The 'trapping hypothesis' has only been tested using in vitro systems. However, the long-term trapping of varenicline in GSats in the human brain explains the mystery why the rate of varenicline metabolism is much slower (4-5 days) compared to that of untrapped and rapidly metabolized nicotine (1-2 hours; (Govind, Vallejo et al. 2017). Here, we extended our analysis in vivo using PET imaging in mice. Based on the pKa and α4β2R affinity values (Table 1), we predicted that the α4β2R PET ligand, 2-FA, is trapped in acidic vesicles similar to varenicline, and Nifene would have significantly less trapping. 125I-epibatidine binding in vitro to measure for reduction in α4β2R upregulation as a measure of trapping confirmed that 2-FA is trapped in acidic vesicles similar to varenicline and Nifene displayed little trapping similar to nicotine (Fig. 2D).

Radioligands 2-[^{18}F]FA and [^{18}F]Nifene were chosen based on their slow (2-FA) and fast (Nifene) kinetics of nicotinic receptor binding. Why these differences in kinetics occur was previously unexplained but consistent with our trapping hypothesis. We successfully employed both 2-[^{18}F]FA and [^{18}F]Nifene in PET/CT mouse brain imaging of α4β2Rs, making this study the first to use 2-[^{18}F]FA in mouse models. As observed for studies in human and other animal models, the 2-[^{18}F]FA uptake in the whole brain is much slower than that of [^{18}F]Nifene, peaking at ~50 min vs ~10 min after the intraperitoneal tracer administration (Fig. 3 B-D). This difference also holds true for the clearance of the two ligands from the brain (Fig. 3 B). We observed statistically significant reduction of ligand binding in the whole brains of mice after acute nicotine injections and in the β2-subunit knockout mice, demonstrating that most specific binding sites are found on β2-containing receptors.

Structural differences between 2-FA and Nifene can explain differences in the rates of entry into the brain and initial differences in binding levels (Fig. 3B-D). Both ligands have similar features: a 2-fluoropyridine group, a methoxyether linkage at the 3-position of the pyridine ring, and a secondary nitrogen in the 4-membered azetidine ring in 2-FA and 5-membered 3,4-dehydropyrrolidine ring in Nifene (Fig. 1A). However, the saturated 4-membered ring in 2-FA versus an unsaturated 5-membered ring in Nifene makes 2-FA more basic (pKa >10), while Nifene's unsaturated ring, which can delocalize electron density away from the nitrogen, is less basic (pKa ~9). This difference in pKa renders 2-FA more hydrophilic relative to Nifene. The lower lipophilicity and higher pKa of 2-FA make it less permeable into the brain, due to a lower proportion of available uncharged species to cross the blood brain barrier (BBB), whereas Nifene has a higher proportion of uncharged species which freely crosses into the brain. This difference in permeability is reflected in Fig-3B-D with a high initial uptake of Nifene compared to 2-FA. The higher affinity of 2-FA and a high nonspecific binding component due to the higher pKa also favors binding-rebinding of 2-FA at the receptor sites, further

slowing down the dissociation kinetics. Nifene, with lower affinity and lower pKa can more rapidly equilibrate and dissociate from the receptor sites, thus having a faster clearance rate.

Further analyses showed that two ligands displayed identical regional uptake with the highest uptake within the thalamus and midbrain (Fig. 3A), consistent with PET imaging studies in humans and other animal models (Hillmer, Wooten et al. 2011, Hillmer, Wooten et al. 2012, Hillmer, Wooten et al. 2013, Mukherjee, Lao et al. 2018). Regional binding differences were diminished in AN mice and completely abolished in KO mice (Fig. 3C-D). These findings demonstrate that the ligand uptake in the cerebellum represents mostly non-specific binding. However, the WT mice displayed higher SUVs in the cerebellum compared to AN and KO mice for both 2-[^{18}F]FA and [^{18}F]Nifene, indicating the presence of some ligand specific binding. This cerebellum specific binding signal is not unique to mice, as studies in rats using 2-[^{18}F]FA PET found a nicotine displaceable signal component in this region (Vaupel, Stein et al. 2007). A study using [^{18}F]Nifene in rats also noticed significant ligand displacement in the cerebellum following administration of both lobeline and (-)nicotine, indicating the presence of specific binding (Hillmer, Wooten et al. 2013). Due to the presence of this specific binding signal, DVR calculations using a cerebellum reference region will underestimate the binding potential. Because our study design takes advantage of AN and KO mice whose cerebellar specific binding was completely abolished, only DVR values of the WT mice underestimate the true binding potential. Despite the underestimation, the WT mice displayed significantly higher DVR compared to all other groups, indicating that our choice of reference region was suitable for this application. However, future studies should consider alternative reference regions or measurement of arterial blood for improved PET quantification.

Chloroquine, which is a BBB permeable weak base and not a nicotinic ligand, has been used widely to reduce the pH gradient across intracellular acidic compartments. The decrease of the pH gradient

across intracellular acidic vesicles has been directly measured in cultured cells (Dong, Song et al. 2017). We found that inclusion of chloroquine in the medium at concentrations of 15-150 μM or NH_4Cl at 20 mM significantly reduced trapping of varenicline and 2-FA in cultured cells (Fig. 1D). We assume the reduction in trapping is caused by chloroquine entry in the α4β2R-containing Golgi satellite vesicles reducing the pH through their protonation without interfering with nicotinic ligand binding to α4β2Rs so that weak base nicotinic ligand is less trapped. Comparing the 2-[^{18}F]FA SUV TACs between the CQ mice and the untreated WT mice revealed that chloroquine resulted in uptake of the ligand in the target regions to more closely resemble the cerebellum (evident in Fig. 5 E-F), indicating reduced specific binding in these regions and significantly faster 2-[^{18}F]FA kinetics. Under the presence of chloroquine, regional brain uptake was higher than in the cerebellum, indicative of the presence of specific ligand binding. These results are consistent with 2-[^{18}F]FA being trapped within intracellular acidic vesicles, the Golgi satellites, *in vivo* in the mouse brains.

Of interest is the use of dynamic PET data to measure the efflux rate of 2-FA from the acidic vesicles to compare with the *in vitro* findings. When generating the Logan plots, the tissue-to-plasma efflux rate (k_2') was determined using SRTM with a cerebellum reference tissue. For 2-FA, the efflux rate was determined as 0.033±0.0030 min^{-1} (mean±SEM). Compared to the efflux rate determined for Nifene (0.45±0.084 min^{-1}), 2-FA reveals much slower washout from the brain. Future studies will explore measurement of the arterial blood curve and use of an image derived input function in different compartment models to estimate these rate constants, where the value of k_4 is likely to be a more accurate measure of the efflux of ligand from the intracellular acidic vesicles.

Taken together, our results are consistent with 2-FA and Nifene interacting with α4β2Rs by different mechanisms. Because Nifene does not get trapped significantly in the α4β2R-containing Golgi satellite vesicles its exit from neurons expressing α4β2Rs is only delayed by the binding and unbinding to the

receptors and is a measure of the total α4β2R population, both cell-surface and in intracellular receptors. 2-FA binds to α4β2Rs in the Golgi satellites and becomes trapped for many hours. Because its binding and unbinding to receptors outside the Golgi satellites is so much faster than its exit rate from the Golgi satellites, its PET signal in the brain is a measure of only Golgi satellite pools of receptors. In short, the two ligands measure separate α4β2R features. In this study, we have combined *in vitro* cellular assays with *in vivo* PET and new insights into the changes that occur during nicotine addiction have emerged that could help design more effective anti-smoking drugs. Specifically, our findings suggest that design elements, such as pKa and receptor affinity that regulate trapping in the Golgi satellites, need to be explored in terms of drug design. The same drug design strategy can be applied to other neurological conditions in which nicotinic receptors are implicated such as dementia (Picciotto, Brunzell et al. 2002), depression (Picciotto, Brunzell et al. 2002) and attention deficits (Faraone and Biederman 1998).

References

Agboola, S. A., T. Coleman, A. McNeill and J. Leonardi-Bee (2015). "Abstinence and relapse among smokers who use varenicline in a quit attempt-a pooled analysis of randomized controlled trials." Addiction **110**(7): 1182-1193.

Albuquerque, E. X., E. F. Pereira, M. Alkondon and S. W. Rogers (2009). "Mammalian nicotinic acetylcholine receptors: from structure to function." Physiol Rev **89**(1): 73-120.

Benwell, M. E., D. J. Balfour and J. M. Anderson (1988). "Evidence that tobacco smoking increases the density of (-)-[3H]nicotine binding sites in human brain." J Neurochem **50**(4): 1243-1247.

Bieszczad, K. M., R. Kant, C. C. Constantinescu, S. K. Pandey, H. D. Kawai, R. Metherate, N. M. Weinberger and J. Mukherjee (2012). "Nicotinic acetylcholine receptors in rat forebrain that bind (1)(8)F-nifene: relating PET imaging, autoradiography, and behavior." Synapse **66**(5): 418-434.

Breese, C. R., C. Adams, J. Logel, C. Drebing, Y. Rollins, M. Barnhart, B. Sullivan, B. K. Demasters, R. Freedman and S. Leonard (1997). "Comparison of the regional expression of nicotinic acetylcholine receptor alpha7 mRNA and [125I]-alpha-bungarotoxin binding in human postmortem brain." J Comp Neurol **387**(3): 385-398.

Brown, D. A. and J. Garthwaite (1979). "Intracellular pH and the distribution of weak acids and bases in isolated rat superior cervical ganglia." J Physiol **297**(0): 597-620.

Brown, L., S. Chefer, O. Pavlova, D. B. Vaupel, A. O. Koren, A. S. Kimes, A. G. Horti and A. G. Mukhin (2004). "Evaluation of 5-(2-(4-pyridinyl)vinyl)-6-chloro-3-(1-methyl-2-(S)-pyrrolidinylmethoxy)pyridine and its analogues as PET radioligands for imaging nicotinic acetylcholine receptors." J Neurochem **91**(3): 600-612.

Chattopadhyay, S., B. Xue, D. Collins, R. Pichika, R. Bagnera, F. M. Leslie, B. T. Christian, B. Shi, T. K. Narayanan, S. G. Potkin and J. Mukherjee (2005). "Synthesis and evaluation of nicotine alpha4beta2 receptor radioligand, 5-(3'-18F-fluoropropyl)-3-(2-(S)-pyrrolidinylmethoxy)pyridine, in rodents and PET in nonhuman primate." J Nucl Med **46**(1): 130-140.

Constantinescu, C. C., A. Garcia, M. R. Mirbolooki, M. L. Pan and J. Mukherjee (2013). "Evaluation of [18F]Nifene biodistribution and dosimetry based on whole-body PET imaging of mice." Nucl Med Biol **40**(2): 289-294.

Davila-Garcia, M. I., J. L. Musachio, D. C. Perry, Y. Xiao, A. Horti, E. D. London, R. F. Dannals and K. J. Kellar (1997). "[125I]IPH, an epibatidine analog, binds with high affinity to neuronal nicotinic cholinergic receptors." J Pharmacol Exp Ther **282**(1): 445-451.

Dong, B., X. Song, X. Kong, C. Wang, N. Zhang and W. Lin (2017). "A tumor-targeting and lysosome-specific two-photon fluorescent probe for imaging pH changes in living cells." J Mater Chem B **5**(5): 988-995.

Faraone, S. V. and J. Biederman (1998). "Neurobiology of attention-deficit hyperactivity disorder." Biol Psychiatry **44**(10): 951-958.

Gao, Y., H. Kuwabara, C. E. Spivak, Y. Xiao, K. Kellar, H. T. Ravert, A. Kumar, M. Alexander, J. Hilton, D. F. Wong, R. F. Dannals and A. G. Horti (2008). "Discovery of (-)-7-methyl-2-exo-[3'-(6-[18F]fluoropyridin-2-yl)-5'-pyridinyl]-7-azabicyclo[2.2 .1]heptane, a radiolabeled antagonist for cerebral nicotinic acetylcholine receptor (alpha4beta2-nAChR) with optimal positron emission tomography imaging properties." J Med Chem **51**(15): 4751-4764.

Govind, A. P., O. Jeyifous, T. A. Russell, Z. Yi, A. V. Weigel, A. Ramaprasad, L. Newell, W. Ramos, F. M. Valbuena, J. C. Casler, J. Z. Yan, B. S. Glick, G. T. Swanson, J. Lippincott-Schwartz and W. N. Green (2021). "Activity-dependent Golgi satellite formation in dendrites reshapes the neuronal surface glycoproteome." Elife **10**.

Govind, A. P., Y. F. Vallejo, J. R. Stolz, J. Z. Yan, G. T. Swanson and W. N. Green (2017). "Selective and regulated trapping of nicotinic receptor weak base ligands and relevance to smoking cessation." Elife **6**.

Govind, A. P., P. Vezina and W. N. Green (2009). "Nicotine-induced upregulation of nicotinic receptors: underlying mechanisms and relevance to nicotine addiction." Biochem Pharmacol **78**(7): 756-765.
Govind, A. P., H. Walsh and W. N. Green (2012). "Nicotine-induced upregulation of native neuronal nicotinic receptors is caused by multiple mechanisms." J Neurosci **32**(6): 2227-2238.
Hansch, Corwin and A. Leo (1995). Exploring QSAR: Volume 1: Fundamentals and Applications in Chemistry and Biology.
Hesterman, J., A. Ghayoor, A. Novicki, X. Wang, Y. Cadoret, L. Becerra, R. Gunn and B. Avants (2019). "Multi-atlas approaches for image segmentation across modality, species and application area." Konica Minolta Technology Report **16**: 5.
Hillmer, A. T., D. W. Wooten, M. Farhoud, T. E. Barnhart, J. Mukherjee and B. T. Christian (2013). "The effects of lobeline on alpha4beta2* nicotinic acetylcholine receptor binding and uptake of [(18)F]nifene in rats." J Neurosci Methods **214**(2): 163-169.
Hillmer, A. T., D. W. Wooten, J. M. Moirano, M. Slesarev, T. E. Barnhart, J. W. Engle, R. J. Nickles, D. Murali, M. L. Schneider, J. Mukherjee and B. T. Christian (2011). "Specific alpha4beta2 nicotinic acetylcholine receptor binding of [F-18]nifene in the rhesus monkey." Synapse **65**(12): 1309-1318.
Hillmer, A. T., D. W. Wooten, M. S. Slesarev, E. O. Ahlers, T. E. Barnhart, D. Murali, M. L. Schneider, J. Mukherjee and B. T. Christian (2012). "PET imaging of alpha4beta2* nicotinic acetylcholine receptors: quantitative analysis of 18F-nifene kinetics in the nonhuman primate." J Nucl Med **53**(9): 1471-1480.
Horti, A. G., S. I. Chefer, A. G. Mukhin, A. O. Koren, D. Gündisch, J. M. Links, V. Kurian, R. F. Dannals and E. D. London (2000). "6-[18F]fluoro-A-85380, a novel radioligand for in vivo imaging of central nicotinic acetylcholine receptors." Life Sci **67**(4): 463-469.
Huang, S. C. (2000). "Anatomy of SUV. Standardized uptake value." Nucl Med Biol **27**(7): 643-646.
Karlin, A. (2002). "Emerging structure of the nicotinic acetylcholine receptors." Nat Rev Neurosci **3**(2): 102-114.
Keyes, J. W. (1995). "SUV: standard uptake or silly useless value?" J Nucl Med **36**(10): 1836-1839.
Krishnamoorthy, S., E. Blankemeyer, P. Mollet, S. Surti, R. Van Holen and J. S. Karp (2018). "Performance evaluation of the MOLECUBES β-CUBE-a high spatial resolution and high sensitivity small animal PET scanner utilizing monolithic LYSO scintillation detectors." Phys Med Biol **63**(15): 155013.
Lewis, A. S. and M. R. Picciotto (2013). "High-affinity nicotinic acetylcholine receptor expression and trafficking abnormalities in psychiatric illness." Psychopharmacology (Berl) **229**(3): 477-485.
Logan, J., J. S. Fowler, N. D. Volkow, G. J. Wang, Y. S. Ding and D. L. Alexoff (1996). "Distribution volume ratios without blood sampling from graphical analysis of PET data." J Cereb Blood Flow Metab **16**(5): 834-840.
Lu, H., X. Chen and C. G. Zhan (2007). "First-principles calculation of pKa for cocaine, nicotine, neurotransmitters, and anilines in aqueous solution." J Phys Chem B **111**(35): 10599-10605.
Marks, M. J., J. B. Burch and A. C. Collins (1983). "Effects of chronic nicotine infusion on tolerance development and nicotinic receptors." J Pharmacol Exp Ther **226**(3): 817-825.
Marubio, L. M., A. M. Gardier, S. Durier, D. David, R. Klink, M. M. Arroyo-Jimenez, J. M. McIntosh, F. Rossi, N. Champtiaux, M. Zoli and J. P. Changeux (2003). "Effects of nicotine in the dopaminergic system of mice lacking the alpha4 subunit of neuronal nicotinic acetylcholine receptors." Eur J Neurosci **17**(7): 1329-1337.
Maskos, U., B. E. Molles, S. Pons, M. Besson, B. P. Guiard, J. P. Guilloux, A. Evrard, P. Cazala, A. Cormier, M. Mameli-Engvall, N. Dufour, I. Cloez-Tayarani, A. P. Bemelmans, J. Mallet, A. M. Gardier, V. David, P. Faure, S. Granon and J. P. Changeux (2005). "Nicotine reinforcement and cognition restored by targeted expression of nicotinic receptors." Nature **436**(7047): 103-107.

Mazur, C., B. Powers, K. Zasadny, J. M. Sullivan, H. Dimant, F. Kamme, J. Hesterman, J. Matson, M. Oestergaard, M. Seaman, R. W. Holt, M. Qutaish, I. Polyak, R. Coelho, V. Gottumukkala, C. M. Gaut, M. Berridge, N. J. Albargothy, L. Kelly, R. O. Carare, J. Hoppin, H. Kordasiewicz, E. E. Swayze and A. Verma (2019). "Brain pharmacology of intrathecal antisense oligonucleotides revealed through multimodal imaging." JCI Insight **4**(20).
Mukherjee, J., P. J. Lao, T. J. Betthauser, G. K. Samra, M. L. Pan, I. H. Patel, C. Liang, R. Metherate and B. T. Christian (2018). "Human brain imaging of nicotinic acetylcholine alpha4beta2* receptors using [(18) F]Nifene: Selectivity, functional activity, toxicity, aging effects, gender effects, and extrathalamic pathways." J Comp Neurol **526**(1): 80-95.
Picciotto, M. R., D. H. Brunzell and B. J. Caldarone (2002). "Effect of nicotine and nicotinic receptors on anxiety and depression." Neuroreport **13**(9): 1097-1106.
Picciotto, M. R., M. Zoli, C. Léna, A. Bessis, Y. Lallemand, N. Le Novère, P. Vincent, E. M. Pich, P. Brûlet and J. P. Changeux (1995). "Abnormal avoidance learning in mice lacking functional high-affinity nicotine receptor in the brain." Nature **374**(6517): 65-67.
Picciotto, M. R., M. Zoli, R. Rimondini, C. Lena, L. M. Marubio, E. M. Pich, K. Fuxe and J. P. Changeux (1998). "Acetylcholine receptors containing the beta2 subunit are involved in the reinforcing properties of nicotine." Nature **391**(6663): 173-177.
Pichika, R., B. Easwaramoorthy, D. Collins, B. T. Christian, B. Shi, T. K. Narayanan, S. G. Potkin and J. Mukherjee (2006). "Nicotinic alpha4beta2 receptor imaging agents: part II. Synthesis and biological evaluation of 2-[18F]fluoro-3-[2-((S)-3-pyrrolinyl)methoxy]pyridine (18F-nifene) in rodents and imaging by PET in nonhuman primate." Nucl Med Biol **33**(3): 295-304.
Sallette, J., S. Pons, A. Devillers-Thiery, M. Soudant, L. Prado de Carvalho, J. P. Changeux and P. J. Corringer (2005). "Nicotine upregulates its own receptors through enhanced intracellular maturation." Neuron **46**(4): 595-607.
Schwartz, R. D. and K. J. Kellar (1983). "Nicotinic cholinergic receptor binding sites in the brain: regulation in vivo." Science **220**(4593): 214-216.
Slavine, N. V., P. V. Kulkarni and R. W. McColl (2017). "Iterative Image Processing for Early Diagnostic of Beta-Amyloid Plaque Deposition in Pre-Clinical Alzheimer's Disease Studies." J Appl Bioinforma Comput Biol **6**(2).
Thompson, A. J., S. Metzger, M. Lochner and M. D. Ruepp (2017). "The binding orientation of epibatidine at alpha7 nACh receptors." Neuropharmacology **116**: 421-428.
U.S. Department of Health and Human Services, P. H. S., Office of the Surgeon General. (2014). The Health Consequences of Smoking—50 Years of Progress: A Report of the Surgeon General. .
Valette, H., M. Bottlaender, F. Dolle, I. Guenther, C. Fuseau, C. Coulon, M. Ottaviani and C. Crouzel (1999). "Imaging central nicotinic acetylcholine receptors in baboons with [18F]fluoro-A-85380." J Nucl Med **40**(8): 1374-1380.
Vallejo, Y. F., B. Buisson, D. Bertrand and W. N. Green (2005). "Chronic nicotine exposure upregulates nicotinic receptors by a novel mechanism." J Neurosci **25**(23): 5563-5572.
Vaupel, D. B., E. A. Stein and A. G. Mukhin (2007). "Quantification of alpha4beta2* nicotinic receptors in the rat brain with microPET and 2-[18F]F-A-85380." Neuroimage **34**(4): 1352-1362.
Vezina, P., D. S. McGehee and W. N. Green (2007). "Exposure to nicotine and sensitization of nicotine-induced behaviors." Prog Neuropsychopharmacol Biol Psychiatry **31**(8): 1625-1638.
Vodicka, P., J. Lim, D. T. Williams, K. B. Kegel, K. Chase, H. Park, D. Marchionini, S. Wilkinson, T. Mead, H. Birch, D. Yates, K. Lyons, C. Dominguez, M. Beconi, Z. Yue, N. Aronin and M. DiFiglia (2014). "Assessment of chloroquine treatment for modulating autophagy flux in brain of WT and HD mice." J Huntingtons Dis **3**(2): 159-174.

Tables

Table 1. Nicotinic ligand acidity and affinity for α4β2 receptors.

Compound	**Ki**	**pKa**	**Log P**	Source
Nicotine	5.45 nM (human) [a] 1.68 nM (rat) [b] 1.1 nM [c]	8 [d]	1.17 [e]	a. Mukherjee et al. (2018) b. Pichika et al. (2006) c. This work d. Lu et al. (2007) e. Hansch et al (1995) f. Valette et al. (1999) g. Gao et al. (2008) h. Brown et al. (2004) i. Davila-Garcia et al. (1997) j. Govind et al. (2017) k. Thompson et al. (2017)
Nifene	0.83 nM (human) [a] 0.50 nM (rat) [b] 0.42 nM [c]	9.19 [d]	-0.52 [b]	
2-FA85380	0.08 nM [f] 1.33 nM [g] 0.097 nM [c]	10.5 [d]	-2.09 [h]	
Iodoepibatidine	0.09 nM [i] 0.01-0.05 nM [j]	10.5 [k]	NA	
Varenicline	0.4 nM [j]	9.2 [j]	-0.82	

Table 2. Baseline information of the animals imaged with PET

			WT	KO	AN	CQ
Sample, n	2-[^{18}F]-A85380		10	11	10	6
	[^{18}F]-Nifene		12	7	4	
BW, g		Male	30.5 ± 0.6	30.6 ± 0.8	27.2 ± 2.2	28.7 ± 1.2
		Female	21.6 ± 0.7	21.0 ± 0.5	18.8 ± 0.8	22.3 ± 0.9
Injected dose of 2-[^{18}F]-A85380 (μCi)			192 ± 13	149 ± 13	201 ± 11	137 ± 7
Injected dose of [^{18}F]-Nifene (μCi)			126 ± 7	87 ± 13	152 ± 2	

Figure legends

Figure 1. A. Chemical structures of 2-[^{18}F]fluoro-3-(2(*S*)-azetidinylmethoxy)pyridine and (2-^{18}F-fluoro-3-[2-((S)-3-pyrrolinyl)methoxy]pyridine. **B.** Competition of the ligands, nicotine (black triangle), Nifene (blue square) or 2-FA (red circle), for high affinity binding sites on α4β2Rs as assayed by ^{125}I-epibatidine binding. Live α4β2R-expressing HEK cells were incubated with the indicated concentrations of nicotine, Nifene or 2-FA for 5 min prior to ^{125}I-epibatidine binding. Data are plotted as the fraction of the initial ^{125}I-epibatidine bound to intact cells in the absence any added ligands. Each point is the mean ± SEM. **C.** Trapping of 2-FA and not Nifene in intact α4β2R HEK cells. Cells were treated for 17 hours with Nicotine (10 μM), Nifene (100 μM), 2-FA (100 μM) or varenicline (30 μM) and ^{125}I-epibatidine binding performed on live cells (n = 3). Specific epibatidine binding was represented as % of binding relative to nicotine treated cells. **D.** Loss of trapped 2-FA by disrupting intracellular pH gradient. α4β2R HEK cells were treated with 2-FA and varenicline for 17 hours. Cells were either washed with PBS or exposed to agents that raise pH in intact cells like chloroquine (15 μM or 150 μM) or NH_4Cl (20 mM) for 10 minutes. ^{125}I-epibatidine binding was performed and data plotted as in C. Each point is the mean ± SEM, n=3 for 2-FA and n=5 for varenicline. In all the column graphs in (C and D): ***$p<0.05$; ****$p<0.001$ by one-way ANOVA with Bonferroni's multiple comparison test.

Figure 2. A. Nifrorhodamine labeling of primary cortical cultures expressing α4β2Rs. Cultured neurons (DIV 10) were expressing the Golgi satellite marker St3-GFP (green) and α4 and β2HA subunits. After 24 hours, cultures were treated with 1 μM nicotine for 17 hours. Top panel: cultures were fixed, permeabilized and stained for HA-tagged β2 subunits with anti-HA antibodies (red; secondary antibody anti-mouse Alexa 568). Bottom panels: cultures were labeled with 25 μM Nifrorhodamine (red) for 30 minutes and imaged live. Scale bar, 10 μm. **B.** Nifrorhodamine labeling of dendrites of neurons expressing St3-GFP (green) and α4 and β2-HA subunits (red). HA-tagged β2

subunits are labeled with anti-HA antibodies (left panel, red) after permeabilization and fixation. Nifrorhodamine labeling is displayed in the middle panel (red). The pH-sensitive dye, pHrodo, staining is displayed in the right panel (red). Golgi satellites are displayed in each panel by St3-GFP or St3-Halo expression (green). Arrows mark Golgi satellites with co-labeling for β2-HA subunits (left), Nifrorhodamine (center) and pHrodo (right). Scale bar, 10 μm.

Figure 3. Binding and disassociation of 2-[^{18}F]FA to α4β2Rs is slower than [^{18}F]Nifene. **A.** Brain images of 2-[^{18}F]FA and [^{18}F]Nifene binding at coronal, sagittal, and transverse sections in WT mice. **B.** Whole brain time active curves show [^{18}F]Nifene has faster binding kinetics compared to 2-[^{18}F]FA. The insert compares both tracers after signal normalization to their highest binding respectively. **C & D.** Acute nicotine administration and β2-subunit knockout diminish the binding of 2-[^{18}F]FA & [^{18}F]Nifene.

Figure 4. TACs of 6 brain regions shows that the thalamus and midbrain have the highest α4β2R ligand binding while the cerebellum represents non-specific binding. **A.** TACs of [^{18}F]Nifene in 6 selected brain regions of WT mice. **B.** TACs of [^{18}F]Nifene in KO mice. **C.** TACs of [^{18}F]Nifene in AN mice. **D & E.** Nifene DVR in the thalamus and midbrain of WT, KO and AN mice. KO and AN mice show reduced specific binding compared to WT mice.

Figure 5. *In vivo* CQ treatment decreases the binding of 2-[^{18}F]FA and slows its disassociation in 6 selected brain regions. **A.** TACs of 2-[^{18}F]FA in 6 selected brain regions from WT mice. **B.** TACs of 2-[^{18}F]FA in KO mice. **C.** TACs of 2-[^{18}F]FA in AN mice. **D.** TACs of 2-[^{18}F]FA in chloroquine (CQ) treated WT mice. **E & F.** Binding ratios of each brain region to the cerebellum from WT mice and mice treated with CQ. **G & H.** 2-[^{18}F]FA DVR in the thalamus and midbrain of WT, KO, AN and CQWT mice. KO, AN and CQWT mice have reduced specific binding compared to WT mice.

A.

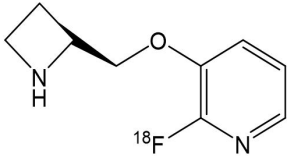

2-[^{18}F]fluoro-3-(2(*S*)-azetidinylmethoxy)pyridine, 2- [^{18}F]A85380 (2-[^{18}F]FA)

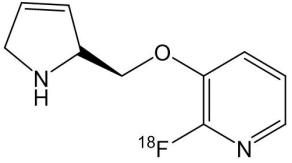

(2-^{18}F-fluoro-3-[2-((S)-3-pyrrolinyl)methoxy]pyridine, ([^{18}F]Nifene)

B.

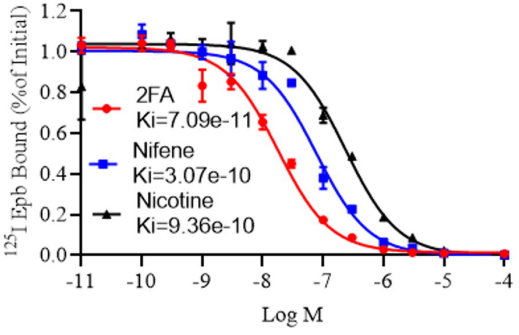

C.

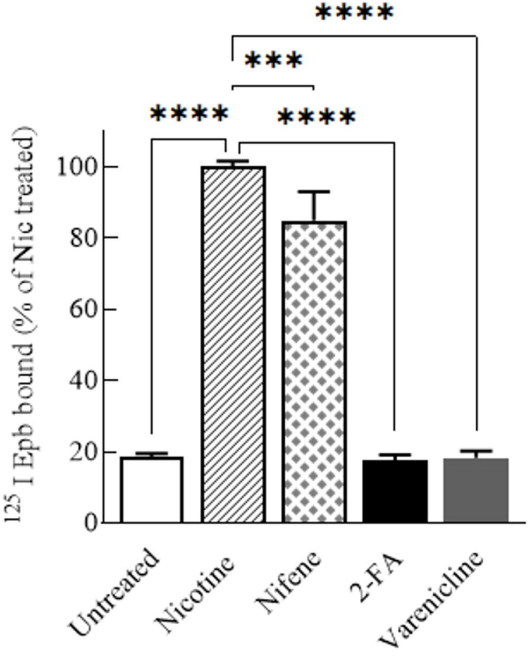

D.

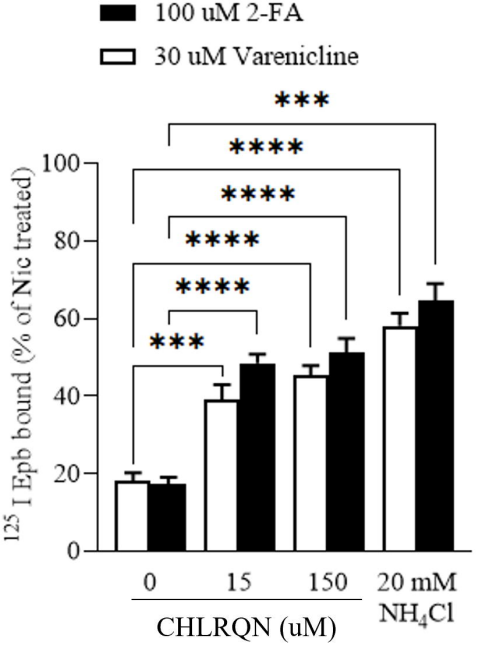

A.

Cultured Neurons

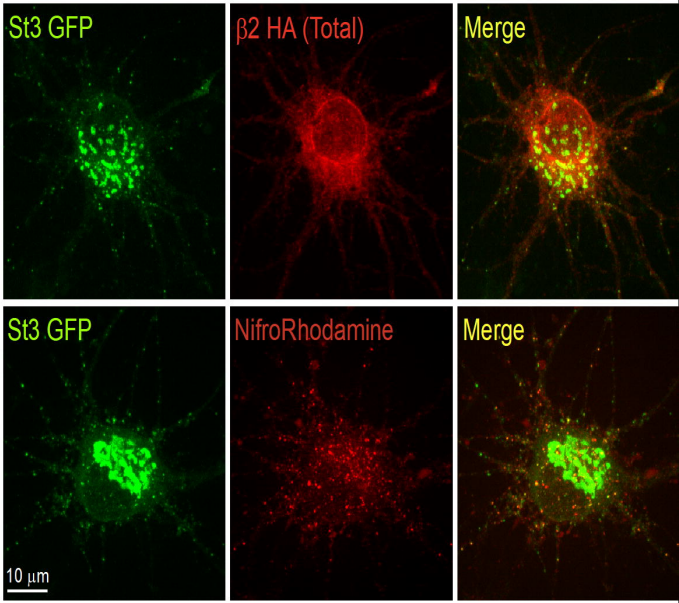

B.

Cultured Neurons (Dendrites)

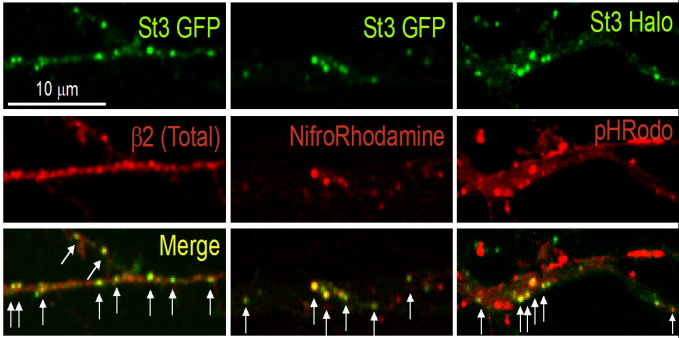

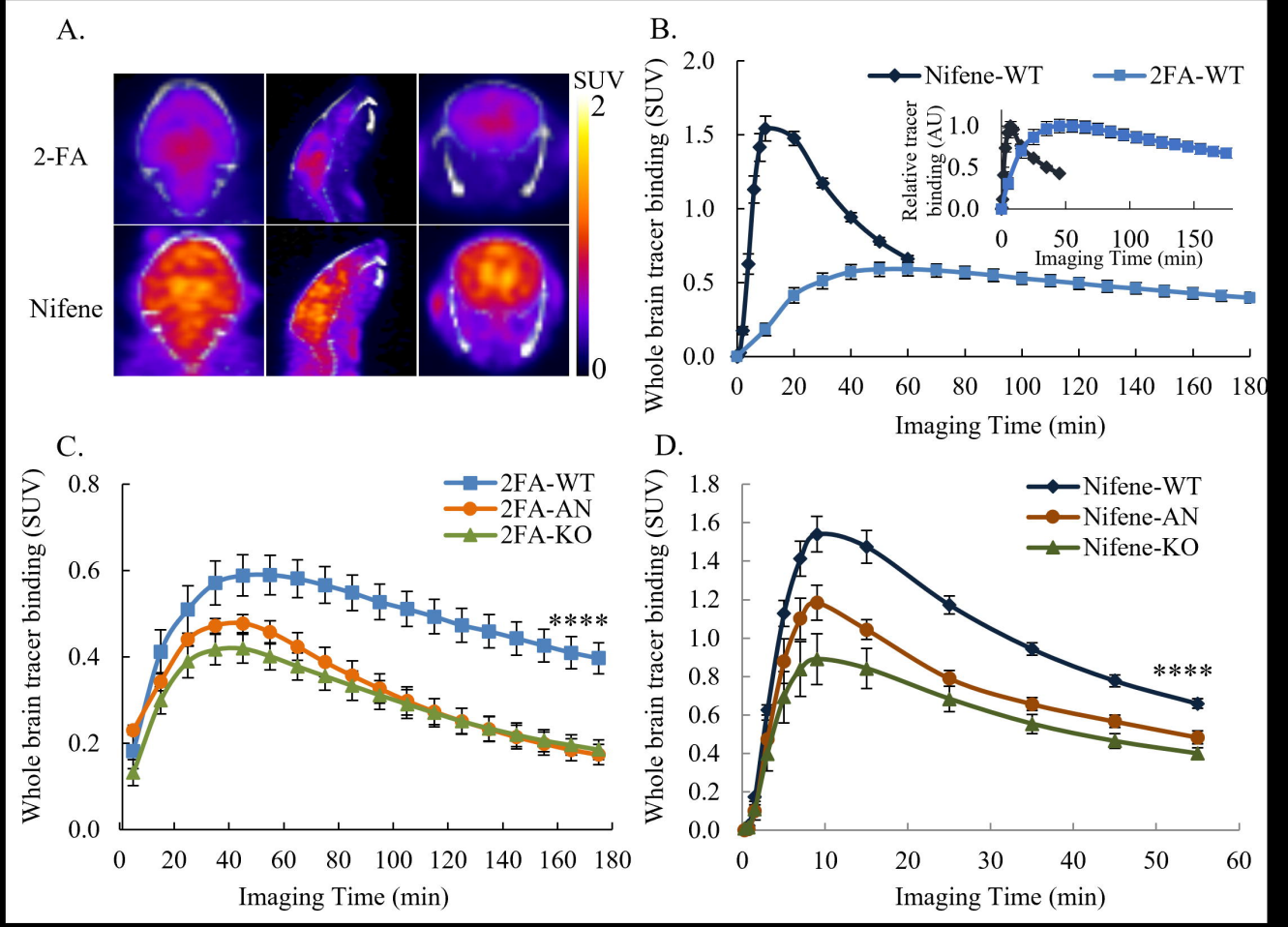
A.
2-FA
Nifene
SUV
2
0
B.
Nifene-WT
2FA-WT
Whole brain tracer binding (SUV)
Imaging Time (min)
Relative tracer binding (AU)
Imaging Time (min)
C.
2FA-WT
2FA-AN
2FA-KO
****
Whole brain tracer binding (SUV)
Imaging Time (min)
D.
Nifene-WT
Nifene-AN
Nifene-KO
****
Whole brain tracer binding (SUV)
Imaging Time (min)

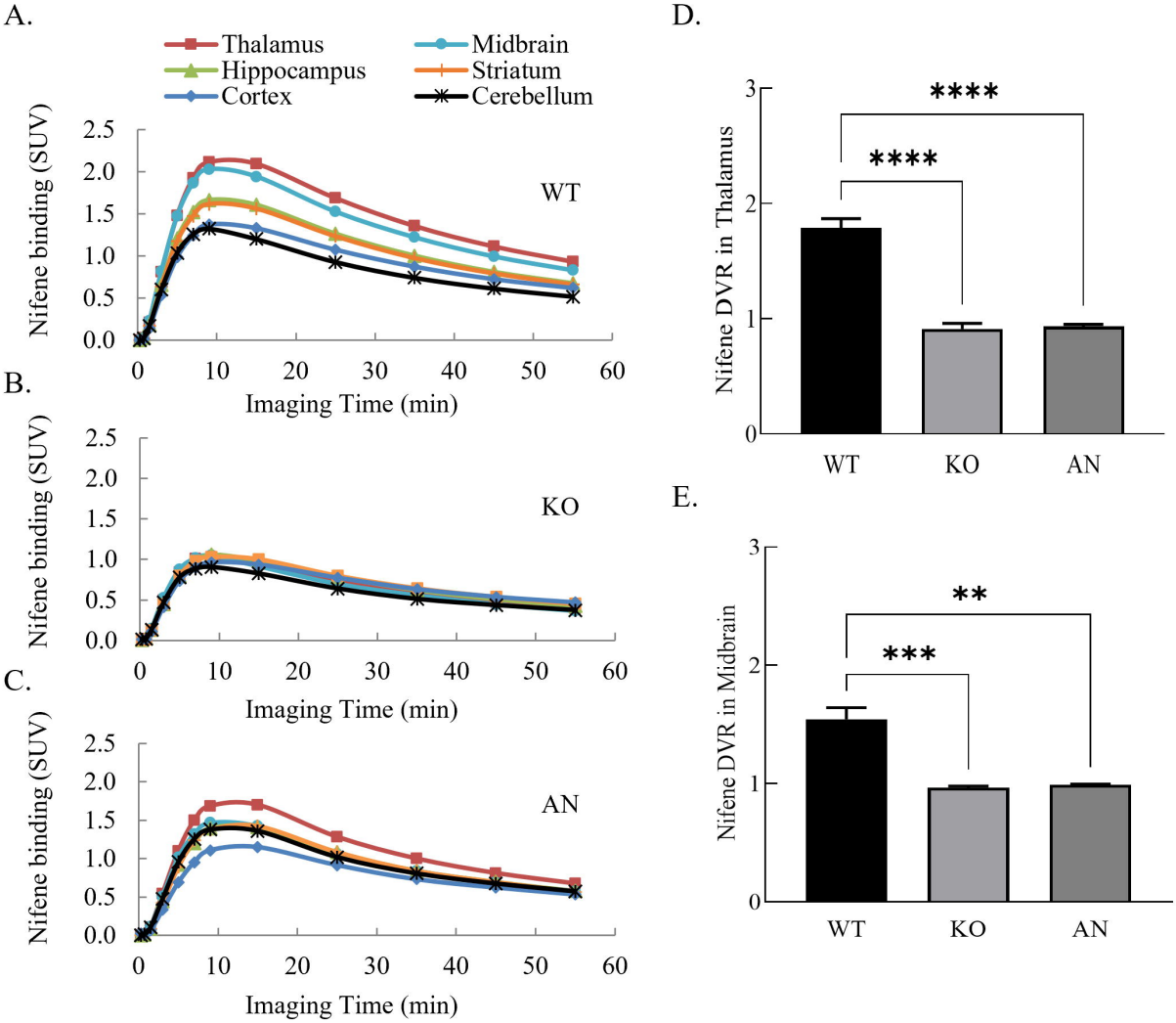
A.
Thalamus
Midbrain
Hippocampus
Striatum
Cortex
Cerebellum
Nifene binding (SUV)
2.5
2.0
1.5
1.0
0.5
0.0
WT
0
10
20
30
40
50
60
Imaging Time (min)
B.
Nifene binding (SUV)
KO
Imaging Time (min)
C.
Nifene binding (SUV)
AN
Imaging Time (min)
D.
Nifene DVR in Thalamus
3
2
1
0
****
****
WT
KO
AN
E.
Nifene DVR in Midbrain
**
***
WT
KO
AN

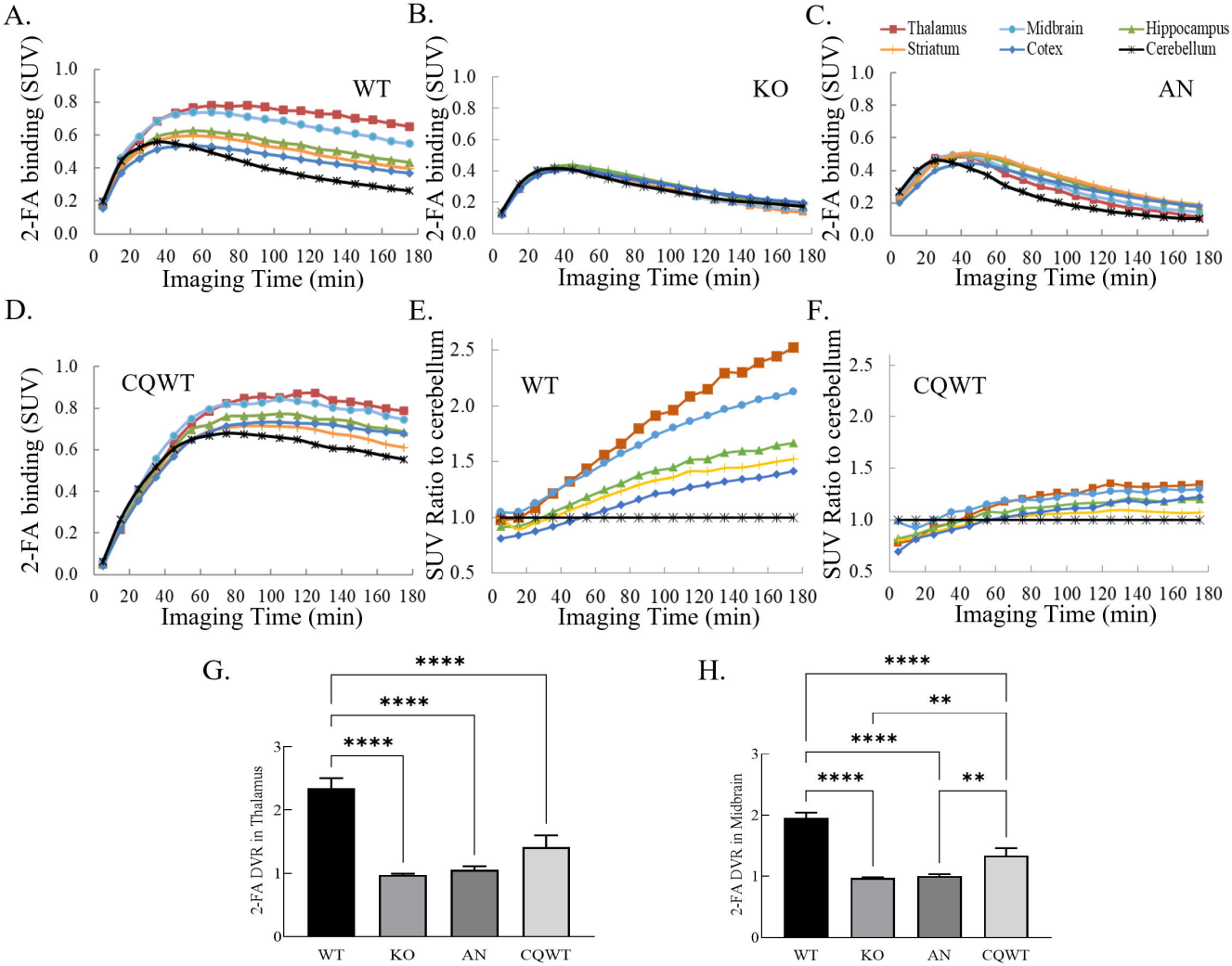
A.
B.
C.
D.
E.
F.
G.
H.
Thalamus
Midbrain
Hippocampus
Striatum
Cotex
Cerebellum
WT
KO
AN
CQWT
2-FA binding (SUV)
SUV Ratio to cerebellum
Imaging Time (min)
2-FA DVR in Thalamus
2-FA DVR in Midbrain
****
**